# Performance Improvement of Rare-Earth Free High-Speed Multilayer IPMSM Using Dual-Phase Magnetic Material

Young-Hoon Jung[1], Ki-O Kim[2], and Myung-Seop Lim[2]

[1]Department of Automotive Engineering, Yeungnam University, Gyeongsan 38541, Republic of Korea
[2]Department of Automotive Engineering, Hanyang University, Seoul 04763, Republic of Korea

**This article proposes the performance improvement of the rare-earth free high-speed multilayer (ML) interior permanent magnet synchronous motor (IPMSM) by using the dual-phase magnetic material (DPMM). To ensure mechanical stability, ML IPMSM should have many bridges. However, in the bridges, a significant leakage flux generates, and due to this, the performance of the motor is decreased. Since the DPMM has magnetic and non-magnetic phases, to solve this problem, the non-magnetic phase is applied to the bridges of ML IPMSM. Through it, the leakage flux is decreased, and the performance improvement of the motor is achieved. In this article, the electrical parameters, torque, and efficiency are compared using finite element analysis (FEA) for the motor with and without the DPMM. Finally, to verify the proposed method, the load test is conducted.**

***Index Terms*— Dual-phase magnetic material (DPMM), ferrite permanent magnet (PM), high-speed multilayer (ML) interior permanent magnet synchronous motor (IPMSM), leakage flux, rare-earth free motor, traction motor for electric vehicle (EV).**

## I. Introduction

RECENTLY, the traction motor of the electric vehicle (EV) is required a high-power density. An interior permanent magnet synchronous motor (IPMSM) using Nd permanent magnet (PM) is the most attractive option to achieve these characteristics [1], but there is a problem of an unstable supply of Nd PM, which is the most important component in the IPMSM using the Nd PM, due to international circumstances [2]. For this reason, various rare-earth free motors have been studied to replace the IPMSM using Nd PM. Among those, the multilayer (ML) IPMSM using ferrite PM can achieve high-power density due to its large reluctance torque. Therefore, in this article, the ML IPMSM using ferrite PM is adopted to replace the IPMSM using Nd PM. However, the ML IPMSM should have a large amount of ferrite PM to secure magnetic torque, which causes mechanical weakness of the ML IPMSM due to centrifugal force at high speed. Therefore, to mechanically ensure stability at high speed, the ML IPMSM inevitably requires many bridges. However, the bridge causes the leakage flux, which decreases the motor performance. To solve this problem, many previous studies have used the optimization technique [3], [4], [5], [6].

In this article, to reduce the leakage flux in the bridge, applying the dual-phase magnetic material (DPMM) is applied to the ML IPMSM. Through this, in this article, it is to examine how the performance is affected when the leakage flux is reduced in the bridge and rib of the rotor of the ML IPMSM by applying the DPMM. The DPMM is a material with magnetic and non-magnetic phases [7]. In the previous studies about the DPMM, only the torque of the synchronous reluctance motor was compared with or without applying the DPMM [7], [8]. In [7] and [8], the torque is increased by applying the DPMM to reduce the leakage flux. Using the same principle, in this article, the performance of the ML IPMSM is improved. To analyze the cause of the performance improvement, the electrical parameter is compared with or without applying the DPMM. Also, the efficiency of the two motors is compared. To ensure the reliability of the analysis results, the test result is compared with the analysis result. To confirm the effect of applying the DPMM, the contents of this article are organized as follows. First, the specification and problem of the target motor to which the DPMM will be applied are introduced. Next, information on the DPMM is briefly introduced. Next, for the motor with or without applying the DPMM, the electrical parameters, torque characteristics, and efficiency are compared using the finite element analysis (FEA). Finally, the test result and FEA result are compared to each other.

TABLE I
Motor Information

| Item | Unit | Value | Note |
|---|---|---|---|
| Maximum torque/power | Nm/kW | 189/120 | - |
| Maximum speed | rpm | 15000 | - |
| Number of poles/slots | -/- | 8/96 | - |
| Stator core material | - | 27PNX1350F | - |
| Rotor core material | - | 35PNT600Y | - |
| Residual induction | T | 0.392 | 100°C |

## II. Rare-Earth Free High-Speed ML IPMSM

In this section, the specification and the problem of the target motor are introduced. The specification and the performance curve according to the rotational speed of the target motor are shown in Table I and Fig. 1, respectively. As shown in Table I, the maximum rotational speed of the target motor is 15 kr/min, which is a high rotational speed for a traction motor. The configuration of the motor is shown in Fig. 2.

Manuscript received 28 March 2023; revised 14 June 2023; accepted 28 July 2023. Date of publication 9 August 2023; date of current version 24 October 2023. Corresponding author: M.-S. Lim (e-mail: myungseop@hanyang.ac.kr).

Color versions of one or more figures in this article are available at https://doi.org/10.1109/TMAG.2023.3303681.

Digital Object Identifier 10.1109/TMAG.2023.3303681

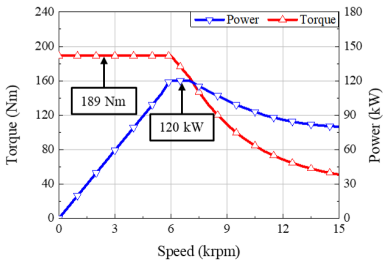


Fig. 1. Power and torque curve according to rotational speed.

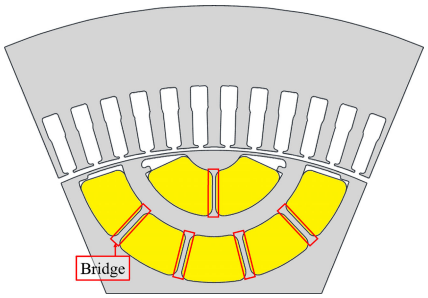


Fig. 2. Configuration of target model.

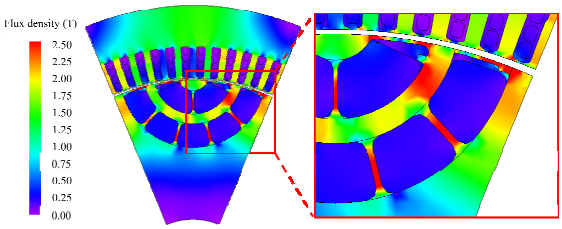


Fig. 3. Leakage flux at bridges and ribs.

TABLE II
MAGNETIC AND MECHANICAL PROPERTIES OF DPMM AND 35PNT600Y

| Item | Unit | DPMM | | 35PNT600Y |
|---|---|---|---|---|
| | | Magnetic | Non-magnetic | |
| Maximum relative permeability | - | 1100 | 1 | 3500 |
| Magnetization saturation | T | 1.5 | 0.25 | 2.0 |
| Electrical resistivity | $\mu\Omega$m | 0.49 | - | 0.59 |
| Young's Modulus | GPa | 200 | 200 | 178 |
| Yield stress | MPa | 275 | 565 | 620 |
| Poisson's ratio | - | 0.28 | 0.259 | 0.3 |

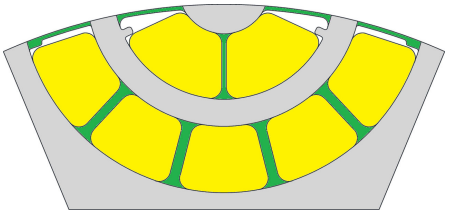

Fig. 4. Rotor configuration applying DPMM.

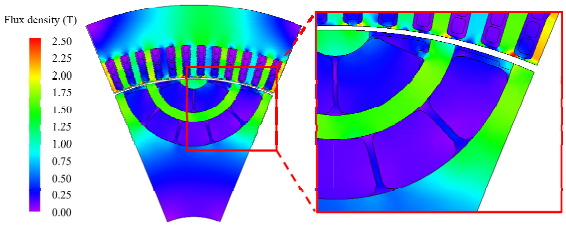


Fig. 5. Leakage flux at bridges and ribs of DPMM model.

As mentioned earlier, it is essential to secure mechanical stability because the target motor is operated at a high speed. For this reason, as shown in Fig. 2, the PM shape is selected as the C-shape because the C-shaped PM has a higher safety factor under the same PM usage than the rectangular-shaped PM [2]. Also, the target motor is designed to have many bridges between the PMs to secure mechanical stability. However, the leakage flux is generated due to these bridges, as shown in Fig. 3, which causes the deterioration of motor performance. Therefore, to improve motor performance, it is necessary to reduce the leakage flux at the bridge. To reduce the leakage flux at the bridges, the optimal design is generally conducted, but the DPMM is used in this article. Section III introduces a brief information on the DPMM used in this article to solve this problem.

## III. Dual-Phase Magnetic Material

As mentioned earlier, DPMM is a DPMM developed by GE and consists of materials with a magnetic phase and a non-magnetic phase [9]. According to [8], DPMM has magnetic and mechanical properties, as listed in Table II. A region with a magnetic phase has a maximum relative permeability of 1100 and magnetization saturation of about 1.5 T, and a region with a non-magnetic phase has a permeability similar to a vacuum. Therefore, in this article, to reduce the leakage flux at the ribs and bridges, the non-magnetic phase is applied to the ribs and bridges of the rotor, which results in improved motor performance. The non-magnetic phase of the DPMM used for ribs and bridges has a yield stress of 565 MPa. Compared to the yield stress of high strength steel 35PNT600Y, it can be seen that the yield stress of the non-magnetic phase of the DPMM is considerably higher. Fig. 4 shows the rotor configuration applying the DPMM. In Fig. 4, a region represented gray and green color is material with the magnetic phase and non-magnetic phase, respectively. Fig. 5 shows the magnetic field distribution of the DPMM model, which is a model to which DPMM is applied. Unlike Fig. 3, there is almost no leakage flux at the ribs and bridges in Fig. 5. Therefore, it can be expected to the motor performance is improved. To confirm the effect of applying the DPMM, the various characteristics of the original and DPMM models are compared in the next section.

## IV. Performance Comparison

In this section, the various characteristics including the torque characteristics, efficiency, and losses of the two motors are compared.

### A. Torque Characteristics

First, the torque characteristics of the two motors are reviewed. In general, to review motor performance, the $d$- and $q$-axes equivalent circuit as in Fig. 6 is used. In the $d$- and

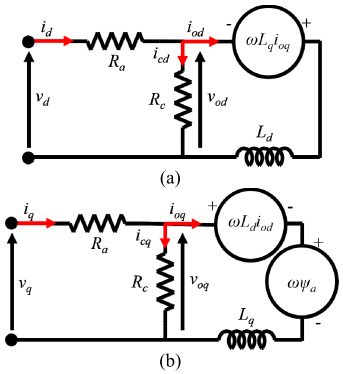


Fig. 6. Equivalent circuit of synchronous motor. (a) $d$-axis. (b) $q$-axis.

$q$-axes equivalent circuit, the output power is expressed as follows:

$$P_{\text{out}} = \begin{bmatrix} v_{\text{od}} & v_{\text{oq}} \end{bmatrix} \begin{bmatrix} i_{\text{od}} \\ i_{\text{oq}} \end{bmatrix} \tag{1}$$

$$\begin{bmatrix} v_{\text{od}} \\ v_{\text{oq}} \end{bmatrix} = \begin{bmatrix} 0 & -\omega_e L_q \\ \omega_e L_d & 0 \end{bmatrix} \begin{bmatrix} i_{\text{od}} \\ i_{\text{oq}} \end{bmatrix} + \begin{bmatrix} 0 \\ \omega_e \psi_f \end{bmatrix} \tag{2}$$

where $P_{\text{out}}$ is the output power; $v_{\text{od}}$ and $v_{\text{oq}}$ are the $d$- and $q$-axes induced voltage, respectively; $i_{\text{od}}$ and $i_{\text{oq}}$ are the magnetizing $d$- and $q$-axes current, respectively; $\omega_e$ is the electrical angular velocity; $L_d$ and $L_q$ are the $d$- and $q$-axes inductance, respectively; $\psi_f$ is the flux linkage by PM. The torque is obtained by dividing the output power by the mechanical angular velocity and expressed as follows:

$$T = \frac{P_{\text{out}}}{\omega_m} = p\{\psi_f i_{\text{oq}} + (L_d - L_q) i_{\text{od}} i_{\text{oq}}\} \tag{3}$$

$$T_m = p\psi_f i_{\text{oq}} \tag{4}$$

$$T_r = p(L_d - L_q) i_{\text{od}} i_{\text{oq}} \tag{5}$$

where $T$ is the torque, $\omega_m$ is the mechanical angular velocity, $p$ is the number of pole pairs, and $T_m$ and $T_r$ are the magnetic and reluctance torque, respectively. As shown in (3), $\psi_f$ and the difference between $L_d$ and $L_q$ are the parameters affecting the torque. Therefore, before examining the torque characteristics according to the application of DPMM, the change of electrical parameters is reviewed. Fig. 7 shows $\psi_f$, $L$, and $L_q$ under the same current condition using the FEA. As shown in Fig. 7, $\psi_f$ of the DPMM model is largely increased compared to the original model, but the difference in the inductances model is smaller in the DPMM model than in the original model. $\psi_f$ of the original model decreases since some of the flux generated by the PM is leaked in the ribs and bridges. On the other hand, $\psi_f$ of the DPMM model is larger than that of the original model since the flux generated by the PM is not leaked in the ribs and bridges.

Based on the previous result, the change in the torque is reviewed. Fig. 8 shows the change in the magnetic, reluctance, and total torque according to applying the DPMM. Since $\psi_f$ of the DPMM model is larger than that of the original model, it is obvious that the magnetic torque of the DPMM is larger than that of the original model. On the other hand, the reluctance torque of the DPMM model is reduced because the difference in the inductances of the DPMM model is smaller than that of

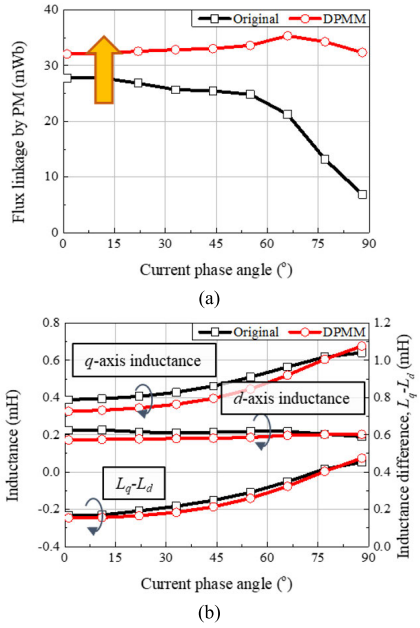


Fig. 7. Electrical parameter comparison under the same current condition. (a) Flux linkage by PM. (b) Inductance.

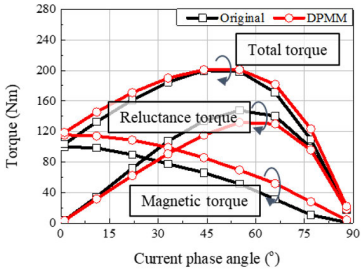


Fig. 8. Torque comparison under the same current condition.

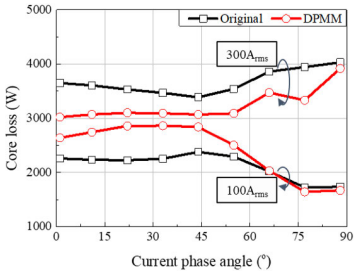


Fig. 9. Core loss comparison according to current magnitude.

the original model. The total torque, which is the sum of the magnetic torque and the reluctance torque, is slightly larger in the DPMM model than in the original model under the same current condition. Conversely, it can be seen that the current magnitude of the DPMM model is smaller under the same torque condition.

### B. Core Loss

In this section, the change in the core loss is introduced according to the application of the DPMM. Since the core loss data of the DPMM are currently difficult to obtain, the core loss data of 35PNT600Y are used as that of the DPMM in this article. Therefore, in this section, only the change in the

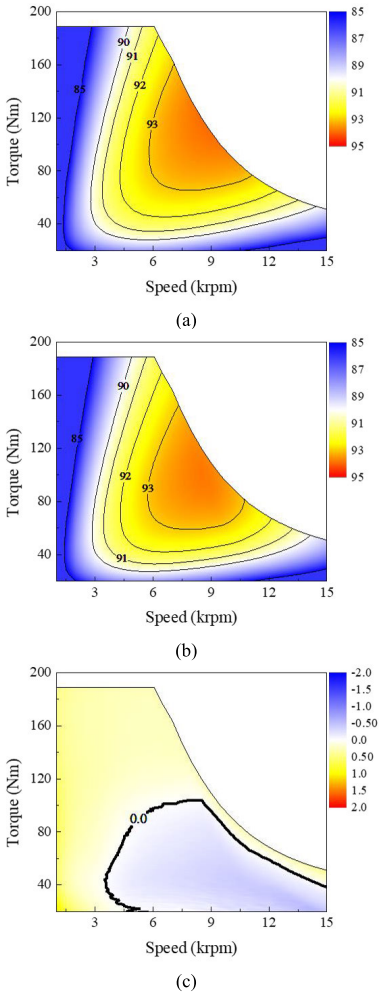


Fig. 10. Efficiency map. (a) Original model. (b) DPMM model. (c) Difference between two models.

core loss due to the magnetic characteristics of the DPMM is presented. Fig. 9 shows the core loss of the two models according to the current magnitude and current phase angle. As shown in Fig. 9, it can be seen that the tendency of the core loss is different according to the current magnitude. For the low current, the core loss of the DPMM model is higher than that of the original model at most current phase angle. Due to the magnetic characteristics of the DPMM, the rotor of the DPMM model reaches the saturation flux density earlier than the original model, which leads to an increase in the core loss of the DPMM model. On the other hand, for the high current, the core loss is lower in the DPMM model compared to the original model. The rotor and stator of the original model have a higher flux density than the DPMM model, which is presented in Figs. 3 and 5, respectively. For this reason, for the high current, the core loss of the original model is higher than that of the DPMM model. Consequently, it can be seen that the higher the current, the lower the core loss of the DPMM model than that of the original model.

### C. Efficiency

Using the previous analysis, the efficiency of the two models is compared. Fig. 10(a) and (b) shows the efficiency map of the two models, respectively. Fig. 10(c) shows the difference in the efficiency map between the two models, which is obtained by subtracting the efficiency of the original model from that of the DPMM model. As shown in Fig. 10(c), the efficiency of the DPMM model is higher than that of the original model in the low-speed regions. Also, in high-speed and high torque regions, the DPMM has a higher efficiency than the original model. To analyze in detail, the difference in the copper and core loss maps of the two models is shown in Figs. 11 and 12, respectively. As shown in Fig. 11, the DPMM model has a lower copper loss than the original model in all operating regions. This is a natural result considering that the torque of the DPMM model is higher than that of the original model under the same current condition, as mentioned in Section IV-A. In Fig. 12, the core loss of the DPMM model is lower than that of the original model in the high torque region. This is because the higher the current, the lower the core loss of the DPMM model than the original model, as described in Section IV-B. If higher power is used at the high-speed region, the efficiency increase area of the DPMM model is expected to be larger.

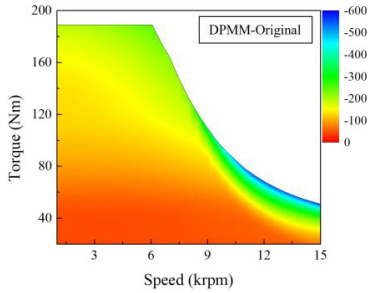


Fig. 11. Copper loss difference map between two models.

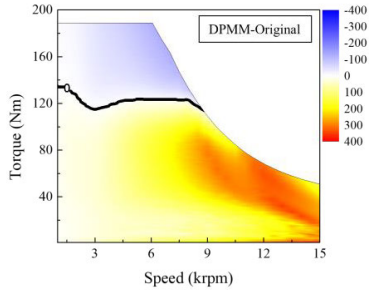


Fig. 12. Core loss difference map between two models.

## V. Verification

To verify the proposed method, it is correct that the DPMM model should be fabricated and tested, but currently, the DPMM model cannot be produced because the DPMM is difficult to obtain. For this reason, in this section, it is tried to indirectly verify the proposed method by ensuring the reliability of the FEA result. To ensure the reliability of the FEA result, the test result of the original model is compared to the FEA result.

Fig. 13(a) and (b) shows the setup of the test and fabricated motor, respectively. As shown in Fig. 13(a), the fabricated motor and load are mechanically connected in series through the torque sensor. Fig. 14 shows the result of the load test.

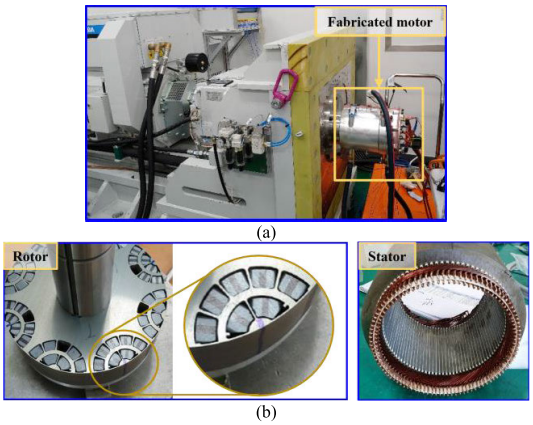


Fig. 13. Test setup and fabricated motor. (a) Test setup. (b) Fabricated motor.

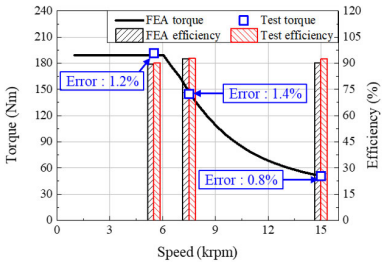


Fig. 14. Load test result.

The load test is conducted at 5.5, 7.5, and 15 kr/min under the maximum torque condition. As shown in Fig. 13, the errors of the torque between the test and FEA are 1.2%, 1.4%, and 0.8%, respectively. Errors at all test points are less than 2%. Also, the efficiency between the two results is similar. Based on those test results, it is confirmed that the result reviewed using FEA in Section IV is reliable. Since the FEA was conducted using the same method for the original and DPMM models, it can be expected that the FEA result of the DPMM model is also similar to the test result. Consequently, it can be concluded that the proposed method is effective in improving the performance of the rare-earth free ML IPMSM.

## VI. Conclusion

In this article, by applying the DPMM, the performance improvement of the rare-earth free high-speed ML IPMSM was proposed. The high-speed ML IPMSM should have many bridges and ribs to be mechanically stable. However, at the bridges and ribs required to ensure the mechanical stability, a significant amount of leakage flux is generated, which causes performance degradation. To solve this problem, the DPMM was applied in this article. Since the DPMM has magnetic phase and non-magnetic phase, the DPMM was applied, so that bridges and ribs have a non-magnetic phase.

Applying the DPMM, the flux linkage by PM of the DPMM model is increased compared to the original model because of decreasing in the leakage flux. As a result, the torque of the DPMM model was higher than the original model. Conversely, the input current required for the same torque is reduced for the DPMM model than for the original model. For the core loss, the DPMM model is lower than that of the original model under the high current condition. Based on those reviewing results, the DPMM model has higher efficiency than the original model in the low-speed region with the low core loss and in the high-speed and high torque region with the high current. Finally, to verify the analysis contents, the original model was fabricated instead of the DPMM model, which is because the DPMM is difficult to obtain. The torque and efficiency were measured through the load test. As a result, the torque errors between the test and FEA results at all test points were less than 2%, and the efficiency of the test result was similar to that of the FEA result. From the test results, it can be confirmed that the FEA results were reliable compared to the test results. Therefore, it can be concluded that the proposed method is suitable for improving the performance of the rare-earth free high-speed ML IPMSM.

## References

[1] Y.-H. Jung, M.-R. Park, and M.-S. Lim, "Asymmetric rotor design of IPMSM for vibration reduction under certain load condition," *IEEE Trans. Energy Convers.*, vol. 35, no. 2, pp. 928–937, Jun. 2020.

[2] Y.-H. Jung, M.-R. Park, K.-O. Kim, J.-W. Chin, J.-P. Hong, and M.-S. Lim, "Design of high-speed multilayer IPMSM using ferrite PM for EV traction considering mechanical and electrical characteristics," *IEEE Trans. Ind. Appl.*, vol. 57, no. 1, pp. 327–339, Jan. 2021.

[3] D.-K. Lim et al., "Analysis and design of a multi-layered and multi-segmented interior permanent magnet motor by using an analytic method," *IEEE Trans. Magn.*, vol. 50, no. 6, Jun. 2014, Art. no. 8201308.

[4] S. Lee, Y.-S. Jeong, Y.-J. Kim, and S.-Y. Jung, "Novel analysis and design methodology of interior permanent-magnet synchronous motor using newly adopted synthetic flux linkage," *IEEE Trans. Ind. Electron.*, vol. 58, no. 9, pp. 3806–3814, Sep. 2011.

[5] L. Fang, S.-I. Kim, S.-O. Kwon, and J.-P. Hong, "Novel double-barrier rotor designs in interior-PM motor for reducing torque pulsation," *IEEE Trans. Magn.*, vol. 46, no. 6, pp. 2183–2186, Jun. 2010.

[6] X. Liang, F. Liu, W. Li, M. Wang, P. Zheng, and Z. Gu, "A novel rotor re-construction method for improving the electromagnetic performance of the interior PMSM," in *Proc. 25th Int. Conf. Electr. Mach. Syst. (ICEMS)*, Chiang Mai, Thailand, Nov. 2022, pp. 1–4, doi: 10.1109/ICEMS56177.2022.9983390.

[7] P. B. Reddy, A. M. El-Refaie, S. Galioto, and J. P. Alexander, "Design of synchronous reluctance motor utilizing dual-phase material for traction applications," *IEEE Trans. Ind. Appl.*, vol. 53, no. 3, pp. 1948–1957, May/Jun. 2017.

[8] P. B. Reddy et al., "Performance testing and analysis of synchronous reluctance motor utilizing dual-phase magnetic material," *IEEE Trans. Ind. Appl.*, vol. 54, no. 3, pp. 2193–2201, May 2018.

[9] L. C. Dial, R. DiDomizio, and F. Johnson, "Dual phase magnetic material component and method of forming," U.S. Patent 9 634 549, Apr. 25, 2017.